ACS OMEGA

http://pubs.acs.org/journal/acsodf

Article

Graphitization and Performance of Deadman Coke in a Large Dissected Blast Furnace

Ziyu Guo, Kexin Jiao,* Jianliang Zhang, Hengbao Ma, Sai Meng, Zhongyi Wang, Jian Zhang, and Yanbing Zong

Cite This: *ACS Omega* 2021, 6, 25430−25439

Read Online

ACCESS | Metrics & More | Article Recommendations

ABSTRACT: The graphitization and performance of deadman coke in the blast furnace hearth have an essential influence on the longevity of the blast furnace. In this paper, coke samples were obtained from various heights in a hearth during the overhaul of the blast furnace. The voidage, particle size, graphitization degree, microstructure, and structure evolution of multiple cokes were analyzed through digital image processing, XRD, Raman spectra, scanning electron microscopy, and energy-dispersive X-ray spectroscopy (SEM-EDS). The graphitization results were compared with feed coke, tuyere coke, cohesive zone coke, and deadman coke in reference, and the main findings were analyzed. The following results were obtained. First, the voidage of deadman coke increased and then decreased with the increase of the depth while the particle size continued to decrease. In addition, the consumption rate of coke as a carburizer, reductant, and heart source was 8.47, 30.95, and 60.58%, respectively. Second, the graphitization degree of deadman coke was extremely high and showed a trend of first increasing and then decreasing. Finally, the evolution mechanism of coke graphitization was proposed. Molten iron, alkali metal, temperature, and mineral were the crucial factors that affect the graphitization of coke. The turning point of the graphitization degree was related to the buoyancy of the hearth.

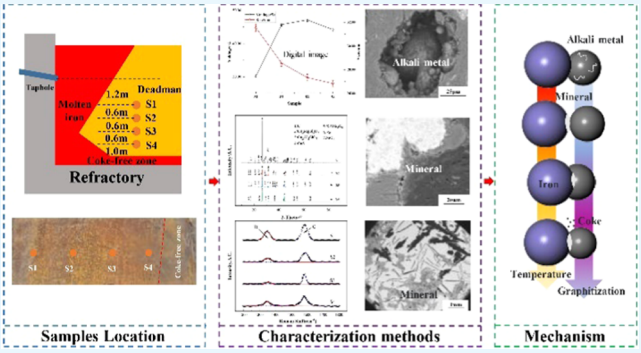

1. INTRODUCTION

CO_2 emission and longevity of a blast furnace have been the topics of most concern for iron-making workers all over the world.[1,2] Coke is one of the important raw fuels of blast furnace iron-making. It takes a long time for coke to be renewed in the blast furnace hearth, so the accumulation of coke for a long time leads to the formation of deadman. The deadman occupies 70% of the volume of the blast furnace hearth.[3,4] The performance of hearth coke directly determines the hearth activity, production capacity, and longevity potential of the blast furnace.[5−9] Therefore, it is necessary to study the performance of the hearth coke, particularly its graphitization degree and consumption pathway. The degree of coke graphitization and consumption pathway are influenced by the target annealing time and temperature, which can reflect the renewal time of the blast furnace.

The graphitization of coke has been investigated extensively by several researchers. In recent years, tuyere-drilling technology has effectively provided coke from the tuyere.[10,11] Therefore, the graphitization of tuyere coke has been studied more intensively. Gupta et al.[12] claimed that the smallest particle size of coke fines (−0.45 mm) has the highest graphitization degree, which was attributed to the fact that tuyere cokes started graphitization from the surface. Some researchers studied the performance of the cohesive zone coke and hearth coke during the overhaul of the blast furnace.[13−15] Chang et al.[16] studied that as the coke is closer to the lower edge of the cohesive, the graphitization degree is higher. Li et al.[17] exported all hearth coke fines and particles that were highly graphitized. They believed that coke graphitization in the high-temperature zone started from the coke surface, which led to the formation of coke fines. Fan et al.[18] studied the microstructure and graphitization of deadman coke obtained in blast furnace hearth dissection. They found that the degree of coke graphitization increased with the deadman descending. Unfortunately, they did not propose an explanation for the graphitization evolution. Li et al.[19] proposed the carbon dissolution−graphite precipitation mechanism to explain the iron catalytic graphitization process by experimentally

Received: June 29, 2021
Accepted: September 8, 2021
Published: September 23, 2021

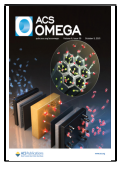

https://doi.org/10.1021/acsomega.1c03398
ACS Omega 2021, 6, 25430−25439

Table 1. Chemical Compositions of Ore, Slag, and Molten Iron, wt %

item	composition							
ore	TFe	Fe_2O_3	FeO	Others				
	57.96	74.71	7.28	18.01				
molten iron	C	Si	Mn	P	S	Fe		
	4.69	0.54	0.07	0.06	0.04	94.60		
slag	CaO	SiO_2	MgO	Al_2O_3	TiO_2	MnO	FeO	S
	43.29	36.25	7.21	11.26	0.47	0.12	0.33	1.07

investigating at 1100, 1200, 1300, and 1500 °C. Coke plays the role of a reductant, carburizer, heat source, and structural support in a blast furnace.[20,21] Unfortunately, the quantitative proportion of the four roles has been less studied. Up to now, the behavior and performance of the hearth deadman coke have not been directly observed and detected. The average service life of a blast furnace is more than 10 years.[22,23] The drilling core sampling is still the only efficient means to obtain the hearth deadman coke and systematically recognize the blast furnace during the blow-off process. Therefore, the understanding of the behavior of blast furnace coke is relatively limited at present, especially the graphitization of hearth coke and coke consumption pathway rate are still major concerns for iron-makers.

Based on previous work, this paper studied the samples of core drilling in the overhaul of a large blast furnace. The voidage, particle size, graphitization degree, microstructure, and structure evolution of multiple cokes were analyzed along with the blast furnace hearth height. The evolution mechanism of coke graphitization and coke consumption pathway rate have been proposed. It provides a reference for further understanding the behavior of the blast furnace.

2. MATERIALS AND METHODS

2.1. Overview of Blast Furnace and Sample Location.

In the present paper, the hearth deadman cokes were obtained during the overhaul of a large commercial blast furnace in China in August 2020. The effective volume of the blast furnace was 4350 m^3. The blast furnace was equipped with 38 tuyeres and 4 tapholes. The blast furnace was put into operation in October 2006 and shut down in June 2020. The blast furnace has been operated at productivity of about 2.14 tHM/(m^3·d). The average coke ratio and pulverized coal injection (PCI) ratio were 330 and 180 kg/tHM, respectively. The average gas utilization rate was 48.92%, and the slag ratio was 242 kg/tHM. The compositions of the ore, slag, and molten iron are shown in Table 1. Ore is mainly composed of FeO, Fe_2O_3, CaO, MgO, Al_2O_3, SiO_2, and so on. Since the calculation in the following chapters mainly used the contents of iron oxide and the iron element, the remaining compositions were replaced by others. It should be noted that the content of TFe represents the content of the iron element in the ore, which can be calculated by the content of FeO and Fe_2O_3. The designed diameter of the hearth is 14.20 m. After the blast furnace was cooled down by water quenching, the hearth was dissected. The sampling location and the sample morphology are presented in Figure 1. The diameter of the corroded hearth was 15.17 m, and the diameter of deadman was 11.95 m. The deadman diameter/hearth diameter ratio was 78.77%. As shown in Figure 1a, the obvious granular cokes were evenly distributed in the deadman. Representative coke samples were obtained by core drilling from hearth deadman during the overhaul period. The diameter of the core drilling coke

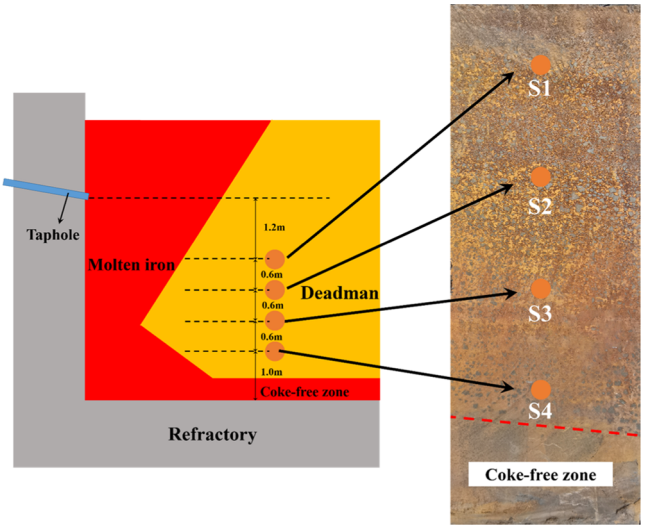

Figure 1. Illustration of sampling position and sample morphology.

samples was 100 mm. The four vertical locations of the coke samples at 1.2, 1.8, 2.4, and 3.0 m below the taphole center level were labeled sequentially as S1, S2, S3, and S4. It should be noted that the area below S4 to the blast furnace bottom was free of coke, which was called the coke-free zone.

2.2. Analysis Methods. Digital image processing is a quick and accurate method to analyze the coke particle size and voidage information. It is a method of characterizing three-dimensional structures in terms of physical two-dimensional domain structures. In other words, it is an unbiased estimate of the volume of a phase in the three-dimensional domain represented by the area fraction of that phase on a random cross section.

The coke samples were cut into two halves along the axis, and cross-sectional area was collected. The cross-sectional size was about 150 × 200 mm. The binary images were acquired from digital camera images using photoshop software, where the black phase represents coke and the white phase represents iron, respectively. The voidage of the deadman and the particle size of the coke were acquired from the binary using photoshop software and Image-Pro Plus (IPP) software, respectively. The voidage and particle size of coke samples were calculated by eqs 1 and 2.[3] It is worth noting that the numerical error of both voidage and particle size is about 1%.

$$\delta = \left(1 - \frac{S_c}{S_t}\right) \times 100\% \quad (1)$$

where δ is the voidage of coke samples (%) and S_c and S_t are the area of coke and the total sample, respectively (mm^2).

$$d = \sqrt{\frac{4S_c}{\pi}} \quad (2)$$

https://doi.org/10.1021/acsomega.1c03398
ACS Omega 2021, 6, 25430−25439

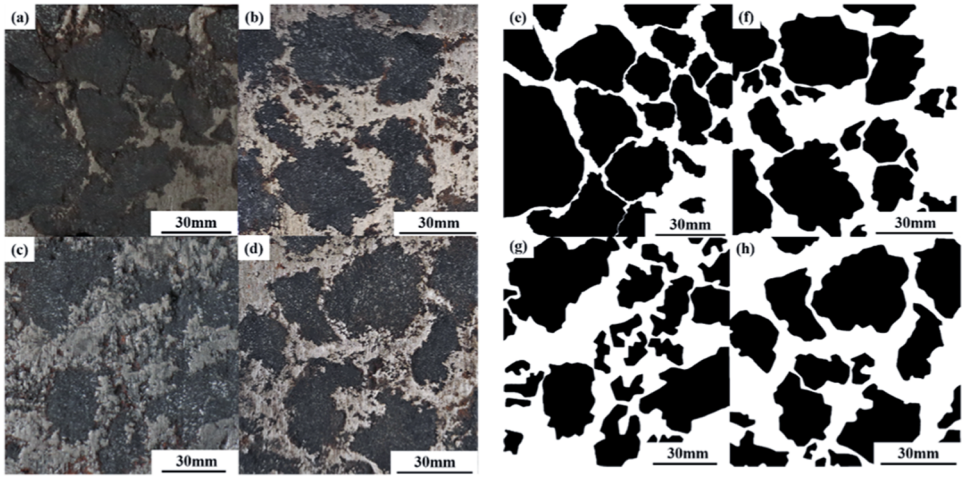

Figure 2. Binary images of deadman coke samples. (a)−(d) Samples morphology of S1, S2, S3, and S4. (e)−(h) Binary images of S1, S2, S3, and S4.

where d is the average coke diameter (mm).

The coke samples were ground with an agate mortar, and the powder particles were collected for X-ray diffraction examination (XRD Ultima IV; Rigaku). The XRD patterns were collected by recording the scatting intensities of coke samples and the scanning angles were from 5 to 90° (2θ) at a scan rate of 10°/min. The coke samples were placed in circular plastic containers with 25 mm diameter with epoxy resin under dry conditions. Surfaces were ground on seven different grades of silicon carbide paper (400, 600, 800, 1000, 1200, 1500, and 2000) and polished with diamond paste. After drying, the surface of the coke samples was coated with gold. Then, the samples were analyzed with a Quanta 250 environmental scanning electron microscope (SEM) equipped with energy-dispersive X-ray spectroscopy (EDS). Then, the Raman spectra of the coke samples that have been analyzed by X-ray diffraction can also be collected using a high-resolution Raman spectrometer (Lab RAMHR Evolution, HORIBA Jobin Yvon S.A.S., France) at room temperature. The frequency band was from 800 to 3000 cm^{-1}.

The pure coke samples were obtained by melting iron in a horizontal-type electric resistance furnace at 1450 °C. After the detached pure coke was washed and dried, the microstructure was observed.

3. DISCUSSION AND ANALYSIS

3.1. Voidage and Particle Size Distribution. The binary images of the representative deadman samples are shown in Figure 2. There was a special image segmentation tool to distinguish the boundaries of coke particles in the IPP software.[24] As shown in eqs 1 and 2, digital image processing was performed on five images, and the average voidage and the particle size of deadman coke were calculated. As shown in Figure 3, from 1.2 m below the blast furnace taphole to 1.0 m above the bottom, the voidage of the deadman increased and then decreased, and the particle size of deadman coke decreased continuously. It is noteworthy that the rate of particle size reduction decreased gradually.

Particle size distributions of deadman cokes are shown in Figure 4. The particle sizes of S1−S4 were mainly concentrated between 20 and 40 mm. The mass percentage of coke with <10 and >40 mm was the least and most, respectively, in S1. The particle size distribution was relatively uniform in S2. The

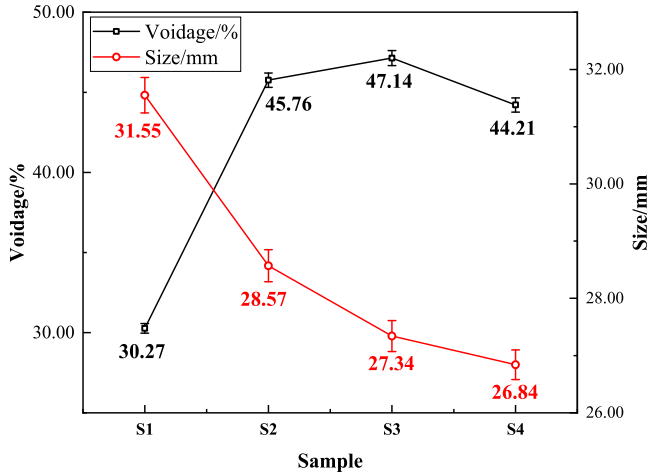

Figure 3. Voidage and particle size of the deadman coke sample.

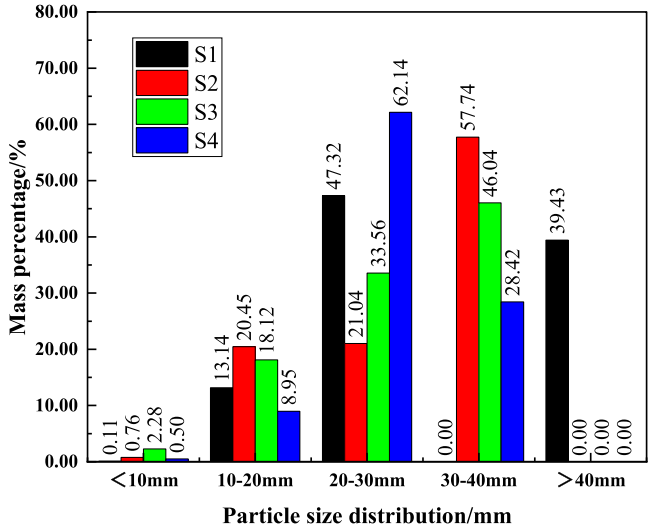

Figure 4. Particle size distribution of deadman coke sample.

particle size of 30−40 mm accounted for the largest in S3. The particle size of <10 and 10−20 mm accounted for a small proportion, and the distribution of 20−30 mm was the most in S4, which was up to 62.14%.

https://doi.org/10.1021/acsomega.1c03398
ACS Omega 2021, 6, 25430−25439

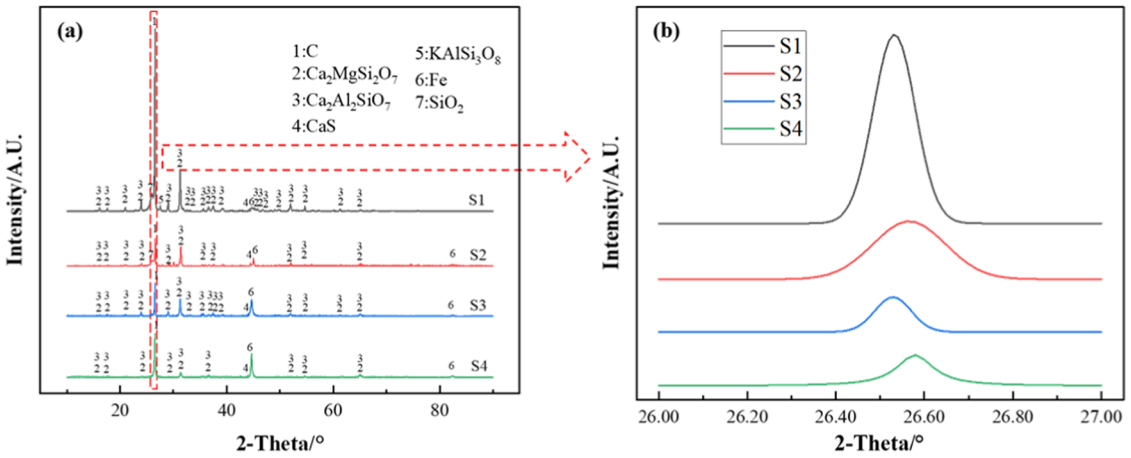

Figure 5. XRD patterns for the coke samples: (a) coke samples and (b) graphite peaks.

The deadman coke particle size and distribution of the hearth cokes were consistent with the results of the previous studies. Niu et al.[25] found that the percentage of hearth particle size of <25 and 25−40 mm were relatively large, and the average size of hearth coke was about 20−31 mm. Zhang et al.[3] also found similar particle size distributions and proposed the average hearth coke sizes of the horizontal samples and vertical samples were 28.04 and 30.55 mm, respectively. As shown in Figure 3, the deadman coke size decreased continuously, which indicates that deadman cokes were constantly carburized. Meanwhile, the slow decreasing rate of particle size was related to the pressure of the upper burden and the buoyancy of the molten iron.[26] Under the comprehensive effect, the deadman floated and sank reciprocally, and the small coke particles at the hearth bottom floated upward and gathered. It can also be obtained from Figure 4, especially the small particles accounted for a large proportion in S4. It was worth noting that some small coke particles may float to the tuyere until they were burned.[27]

$$\eta = \left(1 - \frac{d_{\text{lower coke}}^{3}}{d_{\text{upper coke}}^{3}}\right) \times 100\% \tag{3}$$

where η is the coke consumption rate (%), $d_{\text{lower coke}}$ is the coke diameter in the lower parts of the blast furnace (mm), and $d_{\text{upper coke}}$ is the coke diameter in the upper parts of the blast furnace (mm).

The average particle size of the feed coke was 52.25 mm. The particle size of coke decreased by 39.62% from the furnace top to 1.2 m below the taphole center level. Also, the particle size of coke decreased by 14.93% from 1.2 m below the taphole center level to the coke-free zone. Since S4 was sampled close to the coke-free zone, it can be considered that S4 is the lowest coke in the blast furnace. Coke plays four roles in blast furnace iron-making. It is considered that carburizing of molten iron mainly occurs in the coke below the taphole, and the reductant, heat source, and structural support effects of coke mainly occur above the hearth. Interestingly, the coke particle size above the coke-free zone was relatively large and coke not suddenly disappeared after entering the coke-free zone. According to the above analysis, coke can float up the tuyere and be burned off. It should be noted that the heath coke floated to the tuyere should be considered as a heat source to be consumed. The coke consumption rate was shown in eq 3. The coke consumption rate from the furnace top to the coke-free zone minus that from the furnace top to hearth is the coke consumed as a carburizer. The rest is consumed by tuyere burning. Therefore, the coke consumption in the area above the hearth was 77.98%, the carburizing loss was 8.47%, and the tuyere burning loss was 13.55%. As shown in eqs 4−7 and Table 1, the consumption rate of coke as a reductant and heat source was 30.95 and 60.58%, respectively.

$$n_C(\text{Fe}) = \left[\frac{3w(\text{Fe}_2\text{O}_3)}{160} + \frac{w(\text{FeO})}{72}\right] \Big/ \left[\frac{w(\text{TFe})}{56}\right] \tag{4}$$

$$n_C(\text{Si, Mn, P, S}) = \left[\frac{2w(\text{Si})}{28} + \frac{w(\text{Mn})}{55} + \frac{2.5w(\text{P})}{31} + \frac{0.001w(\text{S})\cdot U}{32}\right] \Big/ \left[\frac{w(\text{Fe})}{56}\right] \tag{5}$$

$$\eta_{re} = \frac{12\,000[n_C(\text{Fe})\cdot\gamma + n_C(\text{Si, Mn, P, S})]}{56(k_c + k_m)} \times 100\% \tag{6}$$

$$\eta_{\text{heat}} = \eta_{\text{upper}} - \eta_{re} + \eta_{\text{burn}} \tag{7}$$

where n_c(Fe) and n_c(Si, Mn, P, S) are the carbon consumption for the reduction of per mole of iron and the total silicon, manganese, phosphorus, and sulfur (mol), respectively; U is the slag ratio (kg/tHM); η_{re} is the coke consumption rate as a reductant (%); γ is the gas utilization rate (%); k_c and k_m are the coke ratio and pulverized coal injection ratio, respectively; η_{upper} is the coke consumption rate from the furnace top to hearth, (%); η_{burn} is the coke consumption as tuyere burning loss, (%); and η_{heat} is the coke consumption as a heat source (%).

In the process of opening and closing the taphole, the cokes were constantly moving with molten iron. The coke was not connected to each other as shown in Figure 2, and the voids between the cokes were filled with molten iron. The voidage showed a trend of increasing first and then decreasing. The blast furnace hearth was relatively in a closed space, and the amount of coke in the hearth was basically kept at a constant value. Therefore, it is reasonable that coke voidage and particle size showed a roughly opposite trend. The voidage evolution pattern and reasons were basically the same as particle size. Interestingly, the voidage of S3 was the largest, which was located 2.4 m below the taphole. Combined with the fact that there were no particles larger than 40 mm in S3 in Figure 4, it

https://doi.org/10.1021/acsomega.1c03398
ACS Omega 2021, 6, 25430−25439

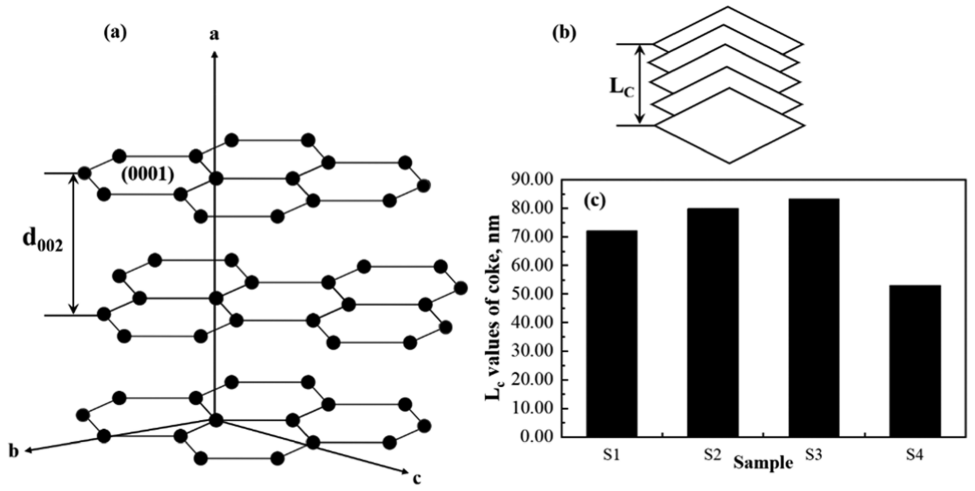

Figure 6. Schematic diagram of d_{002} and L_c, and change in L_c value: (a) schematic of d_{002}; (b) schematic of L_c; and (c) change in L_c value.

may be related to S3 sampling at the corner of the deadman. The circulation of molten iron was relatively high, and the carburization of molten iron was relatively sufficient. It should be noted that the evolution of voidage of deadman coke was also related to the coke graphitization degree.

3.2. Carbon Structure. X-ray diffraction is often used to analyze the coke structure. Previous studies have shown that the peak 002 can represent the coke structure, and the 2θ of peak 002 is in the region from 20 to 30°.[7] The XRD analysis of deadman coke at different positions is shown in Figure 5. Due to the low content of some phases, the XRD spectra did not show diffraction peaks. As shown in Figure 5a, the phase compositions of S1, S2, S3, and S4 were basically similar, and the sharp graphite peak of 002 appeared when 2θ was about 26.5°. The slag phases were all akermanite ($Ca_2MgSi_2O_7$) and gehlenite ($Ca_2Al_2SiO_7$). Interestingly, leucite ($KAlSi_3O_8$) precipitated in S1.

To further investigate the hidden information in the 002 graphitic peak region, the region from 26.0 to 27.0° was analyzed separately, as shown in Figure 5b. The 002 peak of S1 was particularly sharp and had a very high peak intensity. The narrower and sharper the characteristic peak of 002, the higher is the stacking height of graphite microcrystal. That is, the more stable the carbon structure and the more graphitized. The average carbon stacking height (L_c) and the interlayer spacing (d_{002}) are shown in Figure 6.[7] Based on the characteristic peak of 002, the average carbon stacking height, the interlayer spacing, and the average number (n_{ave}) can be calculated using eqs 8−10.[28] The results are shown in Table 2 and Figure 6c.[12,16,28]

$$d_{002} = \frac{\lambda}{2\sin\theta} \tag{8}$$

$$L_c = \frac{0.89\lambda}{B\cos\theta} \tag{9}$$

$$n_{ave} = \frac{L_C}{d_{002}} \tag{10}$$

where λ is the wavelength of the XRD (nm), θ is the diffraction angle of the 002 peak (°), and B is the full width at half-maximum (FWHM) in radians.

Raman spectroscopy is also an effective way to analyze carbon structure. The graphitization degree was characterized by a D peak and a G peak. Previous studies have shown that the D peak and the G peak are near 1350 and 1590 cm^{-1}, respectively, which present as defects and highly graphitic structures, respectively.[29] Therefore, the higher the relative intensity of the G peak, the higher is the graphitization degree. Dong et al.[10] proposed that the intensity of the G peak to the D peak is an indicator of the graphitization degree. In addition, the area ratio of two peaks was also claimed to evaluate the graphitization degree.[29] The Raman spectra and calculated results are shown in Figure 7. The value of I_G/I_D and A_G/A_D first increased and then decreased from S1 to S4.

Table 2. Structure Parameters of Deadman Coke Samples and Cokes in Reference

number	2θ (deg)	d_{002} (nm)	FWHW (deg)	L_c (nm)	n_{ave}
S1	26.53	0.3357	0.112	72.10	214
S2	26.56	0.3353	0.101	79.96	238
S3	26.53	0.3357	0.097	83.25	248
S4	26.58	0.3350	0.152	53.13	158
feed coke	25.69	0.3465	3.488	2.31	7
cohesive zone coke	25.80	0.3450	1.763	4.59	13
tuyere coke	26.03	0.3420	1.186	6.82	20
dead coke	26.15	0.3405	0.522	15.59	46
coke powder	26.29	0.3387	0.2660	30.34	90

As shown in Table 2, it was worth noting that the values of L_c and n_{ave} of the deadman coke samples were far greater than those of the feed coke, the cohesive zone coke, and tuyere coke, indicating an extremely high graphitization degree.[12,16] The results have also appeared in the study of the coke powder on the edge of hearth coke.[28] It indicates that the coke was further carburized by molten iron and preserved in the hearth for a long time. The consumption path of deadman coke was limited; coke can only be consumed by molten iron carburizing. However, the carburizing rate of molten iron in the hearth was very low, and the coke accumulated in the hearth for a long time. The graphitization degree of deadman coke showed a trend of first increasing and then decreasing from 1.2 m below the blast furnace taphole to 1.0 m above the bottom. It can be deduced that the coke graphitization at 3.2 and 2.4 m below the taphole was the lowest and the highest, respectively, which were the coke near the coke-free zone and at a height level of the deadman corner, respectively. This is

https://doi.org/10.1021/acsomega.1c03398
ACS Omega 2021, 6, 25430−25439

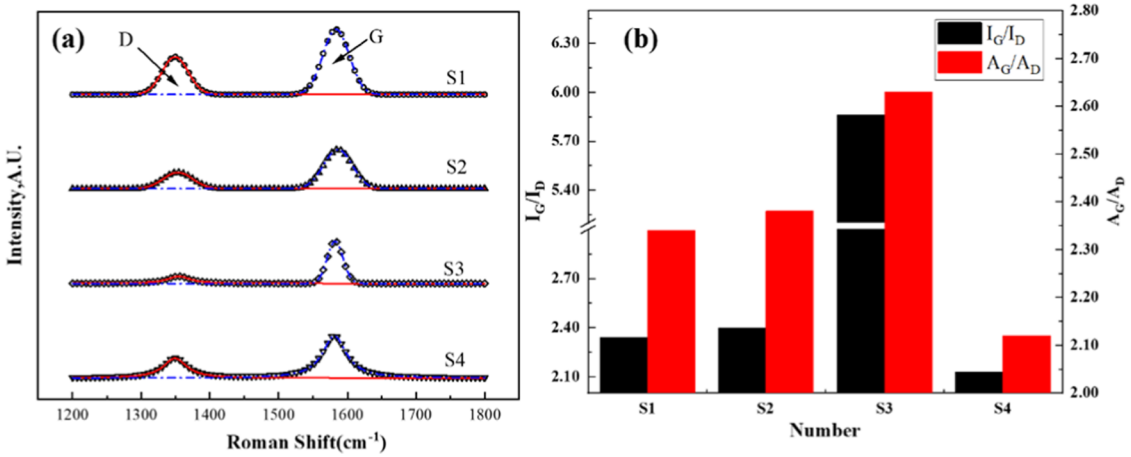

Figure 7. Raman spectrum of the deadman coke samples: (a) trendline and (b) ratio.

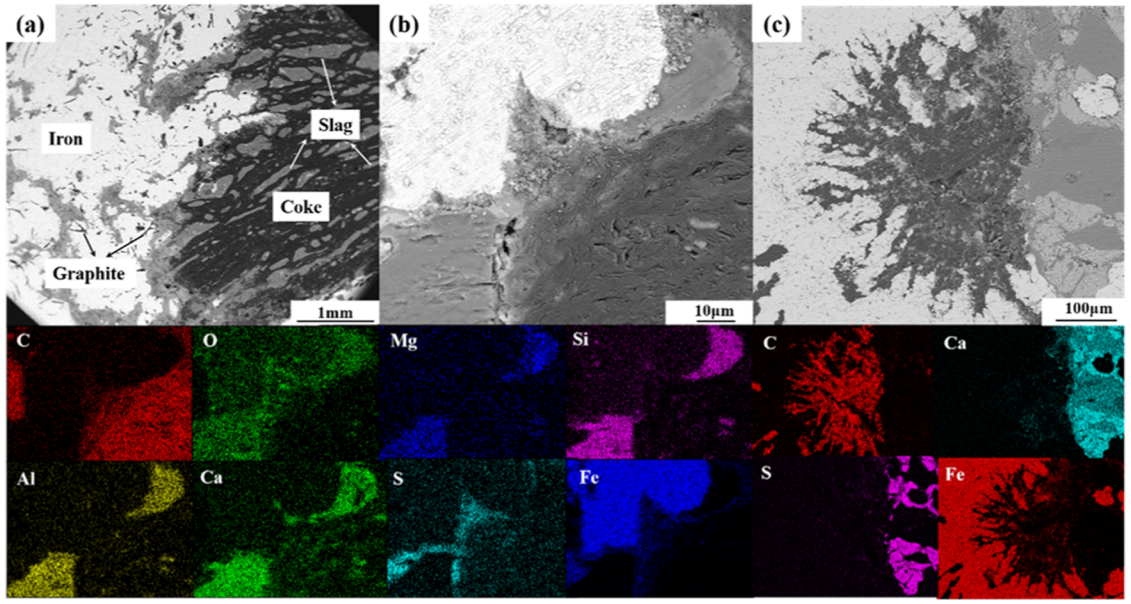

Figure 8. SEM micrographs and EDS maps showing deadman coke: (a) deadman coke samples, (b) interface of coke and the molten iron, and (c) molten iron.

consistent with the Raman results shown in Figure 7. Meanwhile, the stacking height reflected the temperature field distribution of the hearth.[11,30,31] The temperature was one of the most critical factors affecting coke graphitization.

The coke was contacted directly with the molten iron, leading to the carburization reaction. Under the catalysis of the molten iron, the coke was gradually graphitized. Meanwhile, the fact that the higher the graphitization degree of coke, the more difficult it is for carburization, which was different from the previous investigation.[32] The structure of graphite is more stable than that of coke. According to Gibbs energy theory, the more stable the structure, the more demanding the conditions and the less likely the reaction is to occur. The different graphitization of coke was mainly caused by the different contact areas between the coke and the molten iron. The regular hexagonal structure of graphite gave better access to iron than coke. Therefore, the higher the degree of coke graphitization, the more adequate the iron contact and the stronger the iron catalytic effect. Combined with the pattern of voidage and particle size as shown in Figure 3, the larger voidage and smaller particle size meant a more complete iron carburization reaction and stronger iron catalysis. The voidage and particle size of S3 were the largest and relatively small, respectively. It indicates that the contact area of S3 with molten iron was the largest among deadman coke samples.

Interestingly, as deadman coke sank and the carburization reaction continued to occur, and the catalytic effect of molten iron was continually enhanced, the graphitization degree increased as shown in the previous investigation.[18] However, the graphitization degree of S4 was much lower. It may be related to the floating of small particles of deadman coke as mentioned above. Gupta[12] and Li[17] et al. observed that that coke graphitization in the high-temperature zone started from the coke surface and led to the formation of coke fines. The surface of the highly graphitized coke that is catalyzed by the molten iron was washed away. Deadman cokes became small coke particles, which floated under the buoyancy of the lower part of the hearth. The unreacted interior of the coke was exposed. Due to temperature field distribution in the hearth, S4 was at a relatively low temperature. Under the combined effect of temperature and molten iron, the degree of graphitization of S4 was lower than that of upper cokes.

https://doi.org/10.1021/acsomega.1c03398
ACS Omega 2021, 6, 25430−25439

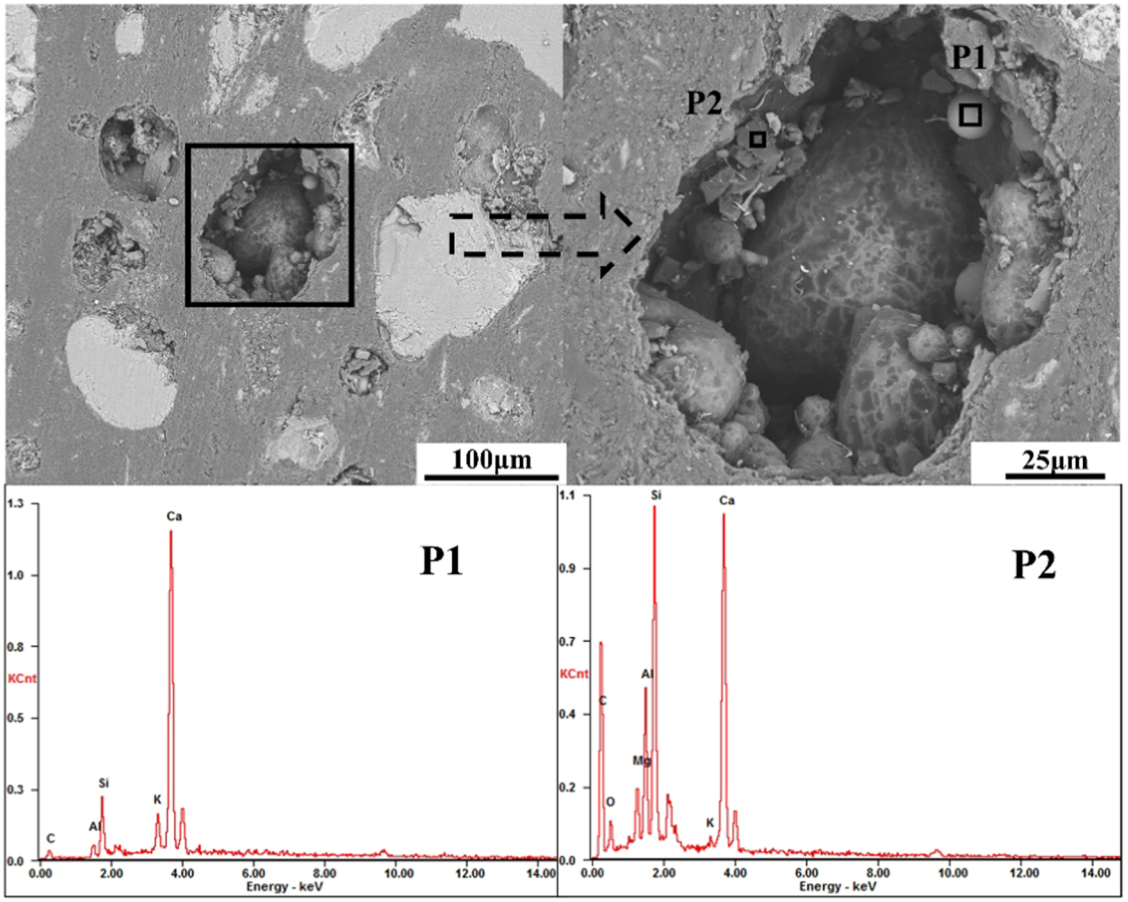

Figure 9. SEM micrographs and EDS maps showing phases in the coke pores in S1.

Table 3. Chemical Compositions of the Samples (wt %)

composition	C	Al_2O_3	SiO_2	MgO	CaO	CaS	K_2O	Na_2O	ZnO
S1	50.88	6.98	17.99	2.59	17.98	2.36	0.82	0.34	0.06
S2	37.22	9.53	18.79	2.81	18.12	12.61	0.58	0.29	0.05
S3	50.14	8.10	15.83	2.81	17.79	4.67	0.44	0.20	0.02
S4	36.05	10.60	19.71	3.76	24.26	5.11	0.25	0.23	0.03

3.3. Micromorphology. The phase composition of the deadman coke samples was the same, only the phase content was different. Therefore, S1 and S3 were taken as representatives for microscopic morphology analysis. The SEM microscopic morphology of S3 is shown in Figure 8. Deadman coke had three main phases, which were white phase, black phase, and gray phase. The EDS analysis of phases showed that the white phase was molten iron, the black phase was coke, and the gray phase was the slag. The network-shaped dark gray phases precipitated as a mineral layer (CaS) at the iron−coke interface, and also existed in the iron phase. The slag phase was present in the coke pores. The morphology of coke pores is shown in Figure 9. There were perfectly spherical and massive phases carrying the K element in the coke pores. The EDS analysis of phases showed that the spherical phases were $Ca_2Al_2SiO_7$, and the massive phases were blast furnace slag.

As shown in Figure 8, the mineral layer at the interface of iron and coke affected direct contact. Due to the presence of coke pores, the coke continuously adsorbed the slag. The coke ash reacted with the final slag of the blast furnace, and the unreacted ash moved with the slag phase. After contact with the molten iron, CaO in the newly formed slag reacted with S in the molten iron to form CaS and CO vapor, as shown in eq 11. The CO vapor evaporated from the blast furnace hearth. The melting point of CaS is about 2673 K (Kelvin). Therefore, the CaS phase adhered to the interface between coke and molten iron as a highly viscose mineral. The desulfurization reaction occurred further and CaS entered the molten iron. This is why minerals were present both at the interface and in the molten iron.

$$(CaO) + (S) + C(s) = CaS(s) + CO(g) \quad (11)$$

The chemical composition of deadman cokes is shown in Table 3. The chemical composition of deadman coke was essentially the same, and K (potassium), Na (sodium), and Zn (zinc) presented in all of them. The composition of deadman coke was significantly different from that of blast furnace slag and original coke. Apart from the CaS phase, the content of Al_2O_3 and CaO in deadman coke was higher than those in the blast furnace slag and original coke, respectively. The phenomenon was caused by the absorption of blast furnace slag by coke pores. It shows that there was enrichment of alkali elements in deadman coke. It is not difficult to observe that the

https://doi.org/10.1021/acsomega.1c03398
ACS Omega 2021, 6, 25430−25439

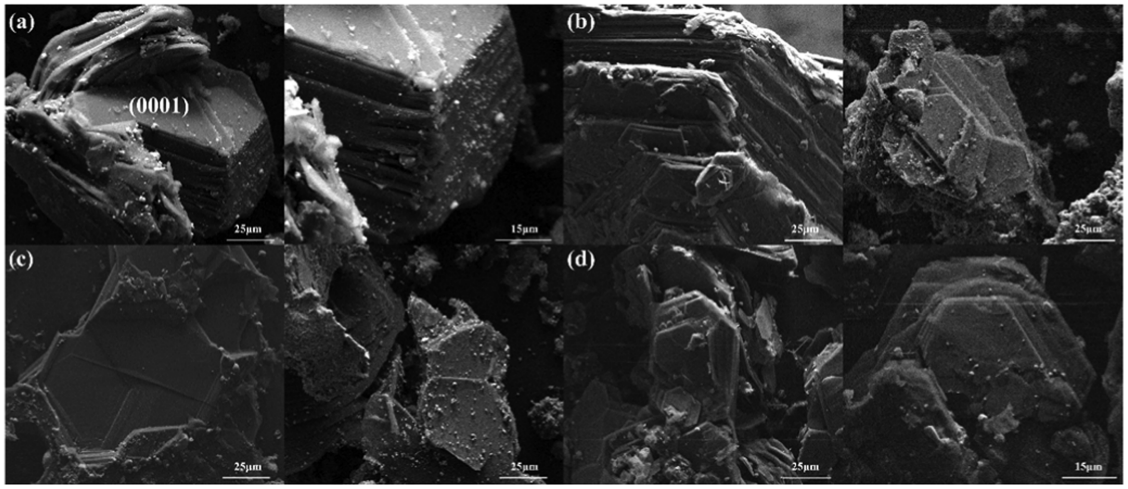

Figure 10. Three-dimensional morphology of coke samples: (a) S1, (b) S2, (c) S3, and (d) S4.

content of K in S1 was the highest. The catalytic effect of alkali elements on coke graphitization has also been claimed in previous studies.[1,33,34] It should be noted that the coke got consumed by reacting with the alkali elements, and its particle size became smaller. The contact area with molten iron was increased and the catalysis of molten iron was promoted. However, alkali metal can also have a detrimental effect on coke. As shown by XRD results, the formation of leucite led to the destruction of the coke structure due to the volume expansion caused by the reaction. Previous studies have shown that this reaction is accompanied by a volume expansion of 15−36%.[35] The three-dimensional morphology of the deadman coke sample is shown in Figure 10. The samples were not polished, the actual microstructure and fracture morphology was reflected. S1, S2, S3, and S4 all showed a layered stacking structure, which indicates that their transition to graphite to different degrees. The twin structure in S1 was caused by the dissociation of the coke structure, which was formed by the detaching, bending, and rolling of the (0001) planes caused by the element K.[36] The twin structure was caused by the symmetry within the crystal. A twin crystal had two or more parts in which the lattice of one part was different from that of the other but was symmetrically oriented. In addition, the hexagonal prism of flake coke was relatively complete in S3. The flake coke showed a nonstandard elongated hexagonal shape, and the overall was hexagonal dipyramid structure, which reflects an inevitable slip between the S2 and S4 layers. It should be noted that the three-dimensional morphology of deadman cokes has a great relationship with their own graphitization degree.

As shown in Figure 9, element K in deadman coke was usually present in the blast furnace slag, indicating that the harmful elements of the hearth deadman coke originated from the blast furnace slag. With the continuous updating of the deadman and the movement of the coke, the harmful elements were transferred to the blast furnace bottom and the edge of the hearth in the height and radial direction with the coke as a medium. It provided a source for harmful element erosion of the hearth sidewall and bottom refractory material.

3.4. Evolution Mechanism of Coke Graphitization. As shown in Figure 11, the mechanism of coke graphitization and performance evolution from 1.2 m below the blast furnace taphole to 1.0 m above the bottom was proposed. Because the upper cokes were close to the slag layer, a large amount of slag

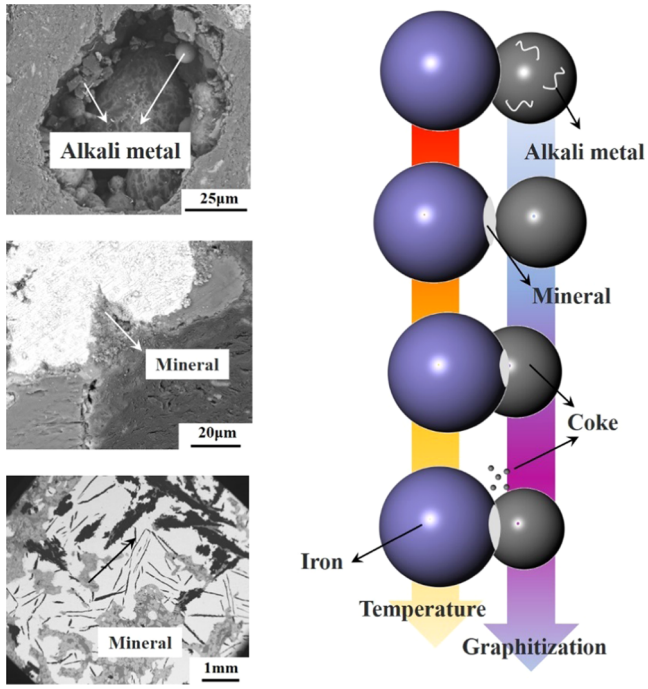

Figure 11. Evolution mechanism of coke graphitization and performance.

containing alkali elements was adsorbed in the pores. The upper cokes were dissociated by alkali elements, which showed a twin structure. In addition, the cokes were catalyzed by molten iron. After the cokes dropped, the CaO in the slag in the coke pores reacted with the coke ash and molten iron to form a mineral (CaS). The mineral adhered to the interface between the molten iron and coke. The coke continued to be catalyzed by molten iron. Afterward, the cokes dropped to the corner of the deadman. The molten iron velocity increased under the effect of the molten iron circulation scouring. Some minerals were washed away by the molten iron, and the contact area between the iron and the coke increased. The cokes were further catalyzed by molten iron, which presented a high graphitization degree. Finally, the cokes dropped to the bottom of the blast furnace, where the temperature in the hearth was relatively low. The highly graphitized coke surface that catalyzed by the upper molten iron was washed away and

https://doi.org/10.1021/acsomega.1c03398
ACS Omega 2021, 6, 25430−25439

formed small coke particles, which floated under the buoyancy of the blast furnace bottom. The unreacted interior of the coke was exposed. Under the combined effect of temperature and molten iron, the graphitization degree of cokes was lower than that of the upper cokes.

4. CONCLUSIONS

The voidage, particle size, graphitization degree, microstructure, and structure evolution of multiple cokes were analyzed through Digital image processing, XRD, Raman spectra, and SEM-EDS. Based on the analysis results of hearth deadman from 1.2 m below the blast furnace taphole to 1.0 m above the bottom, the graphitization evolution mechanism and consumption pathways rate were proposed. The quantitative effects of molten iron and temperature on coke graphitization need to be further analyzed. The main conclusions are summarized as follows:

(1) The voidage of coke increased and then decreased from the deadman top to bottom, and the particle size continued to decrease. The consumption rate of coke as a carburizer, reductant, and heart source was 8.47, 30.95, and 60.58%, respectively.

(2) The graphitization degree of deadman coke samples were far greater than that of the feed coke, the cohesive zone coke, tuyere coke, and deadman coke in references. The graphitization degree of deadman coke increased first and then decreased. The graphitization of coke near the coke-free zone and at a height level of the deadman corner was the lowest and the highest, respectively.

(3) Molten iron, alkali metal, and temperature were the crucial factors that affect the graphitization of hearth coke. Among them, the catalytic effect of molten iron was the most critical. The dissociation of alkali metal and the catalytic effect of molten iron were responsible for the graphitization of deadman coke in the upper part of the hearth. The strong molten iron catalyst was responsible for the highest degree of coke graphitization at a height level of the deadman corner. The buoyancy of the hearth and low temperature were responsible for the lowest graphitization degree of coke near the coke-free zone.

(4) The slag phase in the coke pores formed a mineral layer with coke ash and molten iron, which prevented the direct contact between molten iron and coke. It had negative effects on the graphitization of hearth coke.

AUTHOR INFORMATION

Corresponding Author

Kexin Jiao − *School of Metallurgical and Ecological Engineering, University of Science and Technology Beijing, Beijing 100083, P. R. China;* orcid.org/0000-0003-3456-0762; Email: jiaokexin@ustb.edu.cn

Authors

Ziyu Guo − *School of Metallurgical and Ecological Engineering, University of Science and Technology Beijing, Beijing 100083, P. R. China;* orcid.org/0000-0002-8389-4729

Jianliang Zhang − *School of Metallurgical and Ecological Engineering, University of Science and Technology Beijing, Beijing 100083, P. R. China; State Key Laboratory of Advanced Metallurgy, University of Science and Technology Beijing, Beijing 100083, P. R. China*

Hengbao Ma − *School of Metallurgical and Ecological Engineering, University of Science and Technology Beijing, Beijing 100083, P. R. China*

Sai Meng − *School of Metallurgical and Ecological Engineering, University of Science and Technology Beijing, Beijing 100083, P. R. China*

Zhongyi Wang − *School of Metallurgical and Ecological Engineering, University of Science and Technology Beijing, Beijing 100083, P. R. China*

Jian Zhang − *School of Metallurgical and Ecological Engineering, University of Science and Technology Beijing, Beijing 100083, P. R. China*

Yanbing Zong − *School of Metallurgical and Ecological Engineering, University of Science and Technology Beijing, Beijing 100083, P. R. China*

Complete contact information is available at: https://pubs.acs.org/10.1021/acsomega.1c03398

Notes

The authors declare no competing financial interest.

ACKNOWLEDGMENTS

This work was financially supported by Important Projects in the Scientific Innovation of Shandong province (2019JZZY010404) and thanks for the support given by Taiyuan Iron and Steel Group Iron Plant.

REFERENCES

(1) Dastidar, M.; Bhattacharyya, A.; Sarkar, B.; Dey, R.; Mitra, M.; Schenk, J. The effect of alkali on the reaction kinetics and strength of blast furnace coke. *Fuel* **2020**, *268*, 117388−117398.

(2) Xu, R.; Zhang, J. Reaction Behavior of Coke in a High Alumina Slag. *ISIJ Int.* **2019**, *59*, 2174−2181.

(3) Zhang, L.; Zhang, J.; Jiao, K.; Zou, Z.; Zhao, Y. Observation of Deadman Samples in a Dissected Blast Furnace Hearth. *ISIJ Int.* **2019**, *59*, 1991−1996.

(4) Shao, L.; Xiao, Q.; Zhang, C.; Zou, Z.; Saxén, H. Dead-Man Behavior in the Blast Furnace Hearth—A Brief Review. *Processes* **2020**, *8*, 1335−1351.

(5) Li, K.; Zhang, J.; Liu, Z.; Wang, T.; Ning, X.; Zhong, J.; Xu, R.; Wang, G.; Ren, S.; Yang, T. Zinc Accumulation and Behavior in Tuyere Coke. *Metall. Mater. Trans. B* **2014**, *45*, 1581−1588.

(6) Zhu, H.; Zhan, W.; He, Z.; Yu, Y.; Pang, Q.; Zhang, J. Pore structure evolution during the coke graphitization process in a blast furnace. *Int. J. Miner. Metall. Mater.* **2020**, *27*, 1226−1233.

(7) Li, K.; Khanna, R.; Zhang, J.; Liu, Z.; Sahajwalla, V.; Yang, T.; Kong, D. The evolution of structural order, microstructure and mineral matter of metallurgical coke in a blast furnace: A review. *Fuel* **2014**, *133*, 194−215.

(8) Huang, J.; Yang, Y.; Cao, Y.; Song, L.; Huang, D. Effect of Iron Particles on the Coke Solution Loss Reaction. *ACS Omega* **2020**, *5*, 25042−25048.

(9) Zhang, W.; Hua, F.; Dai, J.; Xue, Z.; Ma, G.; Li, C. Isothermal Kinetic Mechanism of Coke Dissolving in Hot Metal. *Metals* **2019**, *9*, 470−484.

(10) Dong, S.; Paterson, N.; Kazarian, S.; Dugwell, D.; Kandiyoti, R. Characterization of Tuyere-Level Core-Drill Coke samples from Blast Furnace Operation. *Energy Fuels* **2007**, *21*, 3446−3454.

(11) Park, T.; Ko, K.; Lee, J.; Gupta, S.; Sahajwalla, V.; Kim, B. Coke Size Degradation and Its Reactivity Across the Tuyere Regions in a Large-Scale Blast Furnace of Hyundai Steel. *Metall. Mater. Trans. B* **2020**, *51*, 1282−1288.

https://doi.org/10.1021/acsomega.1c03398
ACS Omega 2021, 6, 25430−25439

(12) Gupta, S.; Ye, Z.; Kanniala, R.; Kerkkonen, O.; Sahajwalla, V. Coke graphitization and degradation across the tuyere regions in a blast furnace. *Fuel* **2013**, *113*, 77−85.
(13) Chang, Z.; Jiao, K.; Ning, X.; Zhang, J. Behavior of Alkali Accumulation of Coke in the Cohesive Zone. *Energy Fuels* **2018**, *32*, 8383−8391.
(14) Chang, Z.; Jiao, K.; Zhang, J.; Ning, X. Insights into Accumulation Behavior of Harmful Elements in Cohesive Zone with Reference to Its Influence on Coke. *ISIJ Int.* **2019**, *59*, 1796−1800.
(15) Chang, Z.; Ning, X.; Zhang, J. Insights into phase and mineral matter of metallurgical coke in cohesive zone. *Fuel* **2019**, *254*, 115707−115717.
(16) Chang, Z.; Jiao, K.; Zhang, J. Graphitization Behavior of Coke in the Cohesive Zone. *Metall. Mater. Trans. B* **2018**, *49*, 2956−2962.
(17) Li, K. J.; Zhang, J. L.; Liu, Y. X.; Barati, M.; Liu, Z. J.; Zhong, J. B.; Su, B. X.; Wei, M. F.; Wang, G. W.; Yang, T. J. Graphitization of Coke and Its Interaction with Slag in the Hearth of a Blast Furnace. *Metall. Mater. Trans. B* **2016**, *47*, 811−818.
(18) Fan, X.; Jiao, K.; Zhang, J.; Ma, H.; Jiang, H.; Yan, B. Coke Microstructure and Graphitization Across the Hearth Deadman Regions in a Commercial Blast Furnace. *ISIJ Int.* **2019**, *59*, 1770.
(19) Li, H.; Zhang, H.; Li, K.; Zhang, J.; Sun, M.; Su, B. Catalytic graphitization of coke carbon by iron: Understanding the evolution of carbon Structure, morphology and lattice fringes. *Fuel* **2020**, *279*, 118531−118540.
(20) Li, Y.; Zhang, J.; Wang, G.; Liang, W.; Zhang, N.; Guo, P. Assessment on the effect of unburned pulverized coal on the properties of coke in blast furnace. *Ironmak Steelmak* **2020**, *47*, 228−237.
(21) Liu, Q.; Yang, S.; Wang, C.; Ji, Y. Effect of carbon solution-loss reaction on properties of coke in blast furnace. *J. Iron. Steel Res. Int.* **2020**, *27*, 489−499.
(22) Sun, M.; Zhang, J.; Li, K.; Guo, K.; Wang, H.; Wang, Z.; Jiang, C. Influence of Structure and Mineral Association of Tuyere-Level Coke on Gasification Process. *Metall. Mater. Trans. B* **2018**, *49*, 2611−2621.
(23) Chang, Z.; Zhang, J.; Ning, X. Phase and mineral behavior of coke in cohesive zone. *Fuel* **2019**, *253*, 32−39.
(24) Jiao, K.; Zhang, J.; Chen, C.; Wu, S.; Liang, L. Analysis of the Deadman Features in Hearth Based on Blast Furnace Dissection by Comprehensive Image-processing Technique. *ISIJ Int.* **2019**, *59*, 16−21.
(25) Niu, Q.; Cheng, S.; Xu, W.; Niu, W.; Mei, Y. Analysis of the Coke Particle Size Distribution and Porosity of Deadman Based on Blast Furnace Hearth Dissection. *ISIJ Int.* **2019**, *59*, 1997.
(26) Guo, Z.; Zhang, J.; Jiao, K.; Gao, T.; Zong, Y.; Zhang, J. Research on low-carbon smelting technology of blast furnace − optimized design of blast furnace. *Ironmaking Steelmaking* **2021**, *48*, 685−692.
(27) Guo, Z.; Zhang, J.; Jiao, K.; Zong, Y.; Wang, Z. Occurrence state and behavior of carbon brick brittle in a large dissected blast furnace hearth. *Steel Res. Int.* **2021**, No. 2100273.
(28) Niu, Q.; Cheng, S.; Xu, W.; Niu, W.; Li, A.; Ma, H.; Zhang, S.; Cao, T. Changes in Microstructure and Chemical Composition of Deadman Coke of a 2800 m3 Industrial Blast Furnace. *ISIJ Int.* **2018**, *58*, 667−676.
(29) Rantitsch, G.; Bhattacharyya, A.; Günbati, A.; Schulten, M.; Schenk, J.; Letofsky-Papst, I.; Albering, J. Microstructural evolution of metallurgical coke: Evidence from Raman spectroscopy. *Int. J. Coal Geol* **2020**, *227*, 103546−103558.
(30) Hu, X.; Sundqvist Ökvist, L.; Ölund, M. Materials Properties and Liquid Flow in the Hearth of the Experimental Blast Furnace. *Metals* **2019**, *9*, 572−584.
(31) Gupta, S.; Ye, Z.; Kim, B.; Kerkkonen, O.; Kanniala, R.; Sahajwalla, V. Mineralogy and reactivity of cokes in a working blast furnace. *Fuel Process. Technol.* **2014**, *117*, 30−37.
(32) Sun, M.; Zhang, J.; Li, K.; Li, H.; Wang, Z.; Jiang, C.; Ren, S.; Wang, L.; Zhang, H. The Interfacial Behavior Between Coke and Liquid Iron: A Comparative Study on the Influence of Coke Pore, Carbon Structure and Ash. *JOM* **2020**, *72*, 2174−2183.
(33) Wang, W.; Wang, J.; Xu, R.; Yu, Y.; Jin, Y.; Xue, Z. Influence mechanism of zinc on the solution loss reaction of coke used in blast furnace. *Fuel Process. Technol.* **2017**, *159*, 118−127.
(34) Li, K.; Zhang, J.; Barati, M.; Khanna, R.; Liu, Z.; Zhong, J.; Ning, X.; Ren, S.; Yang, T.; Sahajwalla, V. Influence of alkaline (Na, K) vapors on carbon and mineral behavior in blast furnace cokes. *Fuel* **2015**, *145*, 202−213.
(35) Niu, Q.; Cheng, S.; Xu, W.; Niu, W. Microstructure and Phase of Carbon Brick and Protective Layer of a 2800 m3 Industrial Blast Furnace Hearth. *ISIJ Int.* **2019**, *59*, 1776.
(36) Gornostayev, S.; Härkki, J. Graphite crystals in blast furnace coke. *Carbon* **2007**, *45*, 1145−1151.

https://doi.org/10.1021/acsomega.1c03398
ACS Omega 2021, 6, 25430−25439